

Air-sea and oceanic heat flux contributions to the heat budget of the northern Gulf of Alaska shelf

Markus A. Janout,^{1,2} Thomas J. Weingartner,² and Phyllis J. Stabeno³

Received 20 August 2012; revised 18 January 2013; accepted 22 January 2013.

[1] We constructed annual cycles of National Centers for Environmental Prediction air-sea fluxes and temporal oceanic heat content change from Seward Line hydrographic surveys to quantify the different contributions to the oceanic heat budget within the Alaska Coastal Current (ACC) on the northern Gulf of Alaska shelf. The deficit between air-sea fluxes and the temporal change in oceanic heat content throughout the cooling season (October–April) varies from ~ 40 to 110 W m^{-2} and is balanced by ocean heat flux convergence. Cross-shelf heat flux convergence is insignificant on annual average, and the nearshore heat budget is likely entirely balanced by the ACC, which resupplies $\sim 15\%$ – 50% of the heat removed by air-sea fluxes during the cooling season. Furthermore, we estimated spatial heat flux gradients and conclude that air-sea fluxes increase from east to west and from offshore to onshore. The cross-shore gradients are governed by wind speed gradients, likely due to ageostrophic nearshore wind events during the cooling season, while the along-shelf heat flux gradients are governed by the occurrence of low-pressure systems in the northern GOA that result in cold northerly winds over the northwestern GOA. These results underline the ACC's role as the dominant oceanic heat source to the northern GOA shelf and further imply an increased cooling rate of the ACC west of the Seward Line. Furthermore, our analysis showed that nearshore regions, particularly waters in the ACC, are subjected to stronger winter cooling than the middle and outer shelves.

Citation: Janout, M. A., T. J. Weingartner, and P. J. Stabeno (2013), Air-sea and oceanic heat flux contributions to the heat budget of the northern Gulf of Alaska shelf, *J. Geophys. Res. Oceans*, 118, doi: 10.1002/jgrc.20095.

1. Introduction

[2] The northern Gulf of Alaska (GOA) shelf is a highly productive ecosystem that supports a diversity of commercial fisheries. This production is related to numerous processes, many of which are linked to the atmosphere. For example, from fall through spring, the Aleutian Low dominates the North Pacific Ocean and is responsible for the predominantly downwelling-favorable winds and the large precipitation rates in the northern GOA [Wilson and Overland, 1986; Stabeno *et al.*, 2004]. Winds and coastal freshwater influxes force the Alaska Coastal Current (ACC) [Royer, 1981; Johnson *et al.*, 1988; Schumacher *et al.*, 1989; Weingartner *et al.*, 2005]. The ACC is the salient circulation feature on the inner shelf and advects organisms and water masses around the GOA

and ultimately into the Bering Sea through passes in the Aleutian Islands.

[3] Ecosystem responses following shifts in ocean climate were observed in the GOA in 1977 and 1989 [Anderson and Piatt, 1999; Hare and Mantua, 2000] and recently in the Bering Sea [Coyle *et al.*, 2011; Hunt *et al.*, 2011]. In the winter of 2006/2007, the northern GOA's three-decade-long warming trend [Royer and Grosch, 2006] was interrupted by the strongest ocean cooling since the early 1970s [Janout *et al.*, 2010]. The cooling coincided with delayed spring blooms and delayed zooplankton development in 2007 and 2008 (Hopcroft, personal communications). Salmon production, which has been used as one indicator of the state of the Northeast Pacific (NEP) ecosystem, appear to be correlated with the Pacific Decadal Oscillation [Mantua *et al.*, 1997], a measure of sea surface temperature variability in the NEP, which in return is related to the North Pacific Index, a measure of the strength of the Aleutian Low [Trenberth and Hurrell, 1994]. However, the northern GOA shelf has a complex three-dimensional circulation, and the heat budget is strongly influenced by stratification due to freshwater runoff and its redistribution by along- and cross-shelf advection and mixing. For example, the recent 2007 cooling coincided with some of the lowest geostrophic velocities on the northern GOA shelf and likely complemented the cooling through reduced along-shelf heat transport [Janout *et al.*, 2010]. Although ocean temperatures substantially influence marine ecosystems, the processes that control

¹Alfred-Wegener-Institute for Polar and Marine Research, Bremerhaven, Germany.

²Institute of Marine Science, University of Alaska, Fairbanks, Alaska, USA.

³NOAA/Pacific Marine Environmental Laboratory, Seattle, Washington, USA.

Corresponding author: M. A. Janout, Alfred-Wegener-Institute for Polar and Marine Research, Am Handelshafen 12, D-27570 Bremerhaven, Germany. (Markus.Janout@awi.de)

temperature variability on this shelf remain largely unquantified. Weingartner *et al.* [2005] quantified physical processes in the ACC and their impact on the nearshore GOA freshwater budget. The aim of this paper is to complement their findings by estimating the relative importance of cross- and along-shelf heat flux convergences in comparison to air-sea heat exchanges on the coastal GOA heat budget. Furthermore, long-term weather records are sparse on the northern GOA shelf, and the National Center for Environmental Prediction (NCEP) reanalysis provides only one grid point (in the cross-shelf direction) on the wide (~150 km) northern GOA shelf, which may not necessarily be an adequate representation of shelf-wide conditions. We therefore investigate atmospheric records for along- and cross-shelf gradients on the northern GOA shelf.

[4] This paper is organized as follows. After describing the data in section 2, we present a climatology of hydrographic parameters and air-sea fluxes in sections 3.1 and 3.2, quantify cross- and along-shelf heat transport in sections 3.3 and 3.4, and then examine gradients in air-sea fluxes in sections 3.5 and 3.6, followed by a summary and discussion in section 4.

2. Data Sets

[5] We used oceanographic data from along the Seward Line (Figure 1), which was occupied up to seven times per year (March, April, May, July, August, October, and December) from 1997 to 2004 as part of the NOAA-NSF-funded NEP-GLOBEC program [Weingartner *et al.*, 2002] and since 2005 with support from the North Pacific Research Board (NPRB) for biannual (May and September) cruises. Salinity values reported herein are based on the Practical Salinity Scale 1978.

[6] Atmospheric parameters (wind speed, air and dew point temperatures, and sea level pressure) recorded from National Data Buoy Center (NDBC) buoys around the northern GOA shelf (Figure 1) were used to compute latent and sensible heat fluxes with the COARE 3.0 algorithm [Fairall *et al.*, 1996, 2003] and then compared with NCEP heat flux estimates [Kalnay *et al.*, 1996] at selected grid points near the Seward Line. We additionally use monthly mean values from the North American Regional Reanalysis (NARR), NCEP’s high-resolution combined model and assimilated data set [Mesinger *et al.*, 2006]. In addition, we used QuikSCAT wind data to estimate cross-shelf Ekman transport. The QuikSCAT wind estimates are from twice daily swaths with daily averaged data available at 25 km resolution. Over the northern shelf, the along-shelf component of the wind is nearly zonal [Royer, 2005], so downwelling-favorable winds are easterly.

[7] We also used monthly coastal freshwater discharge anomalies from the Alaska-British Columbia boundary to 150°W from Royer’s [1982] hydrological model. These discharge anomalies are significantly correlated with upper ocean salinities at GAK1 and the along-shelf baroclinic transport in the ACC between November and May [Weingartner *et al.*, 2005]. Current velocity records, available from October–December 2001 and 2002 as well as from February–April 2002 and 2003 from moored current meters, were used to compute seasonally averaged velocities. Two moorings each were located in the ACC near Seward Line stations 2 and 3 and ~120 km to the southwest near Gore Point (Figure 1), respectively. Hourly measurements were recorded at a maximum of four depths between ~30 and 150 m, using Aanderaa RCM7 and RCM9 current meters. The accuracy for speed and direction of the RCM7 (RCM9) is $\pm 1 \text{ cm s}^{-1}$ and $5^\circ\text{--}7.5^\circ$ ($\pm 0.2 \text{ cm s}^{-1}$ and 5°).

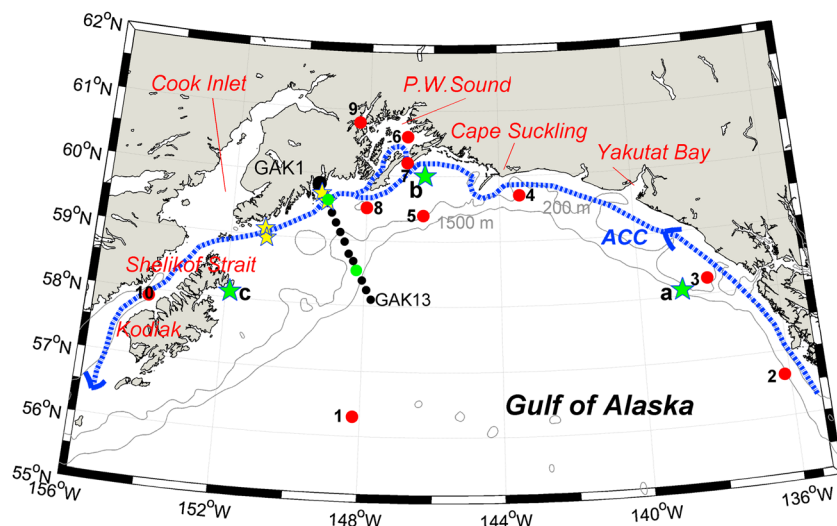


Figure 1. Map of the northern Gulf of Alaska, including the Seward Line (GAK1-13; black dots). The Alaska Coastal Current (ACC) pathway is sketched in blue. The 200 and 1500 m isobaths are based on the General Bathymetric Chart of the Oceans (GEBCO). Mooring locations are indicated by yellow stars. Locations of QuikSCAT data points used in Figure 4 are marked by green dots. NDBC buoys (red dots) used to construct Figure 10: (1) 46001, (2) 46084, (3) 46083, (4) 46082, (5) PAMD, (6) 46060, (7) 46061, (8) 46076, (9) 46081, and (10), 46077. NCEP grid points used in Figure 15 in the (a) eastern GOA, (b) northern GOA, and (c) western GOA are shown by green stars.

The moorings were operated as part of NOAA’s Fisheries Oceanography Coordinated Investigations with deployments and recoveries during May and September cruises.

[8] Observations in the northern GOA provide insufficient spatial coverage to reliably quantify along-shelf heat gradients. We therefore used monthly mean temperature data provided from an ocean reanalysis derived from applying the Simple Ocean Data Assimilation (SODA) methods [Carton and Giese, 2008] in a general ocean circulation model based on the Parallel Ocean Program [Smith et al., 1992]. Horizontal resolution is $0.5^\circ \times 0.5^\circ$, with ~ 10 m vertical intervals in the upper 150 m.

3. Results

3.1. Annual Cycles of Salinity and Temperature Along the Seward Line

[9] We computed seasonal averages of the cross-shelf distribution of salinity (Figure 2) and temperature (Figure 3) along the Seward Line on the northern GOA shelf from about seven annual occupations from 1997 to 2004 by combining March–May transects into a late winter/early spring average, July and August transects represent summer, and October and December form the fall and winter averages, respectively. From fall to spring, salinity primarily controls the density field in the northern GOA [Royer, 2005]. For example, salinity contributes at least 80% to 0–50 m density stratification in the ACC on the inner shelf year-round and from 60% to 90% on the middle and outer shelves from fall to spring. Variations in the density field are thus governed by variability in coastal freshwater runoff and along-shelf (downwelling-favorable) winds (Figure 4) [Weingartner et al., 2005].

[10] Low runoff rates and strong downwelling-favorable winds confine the freshwater to the coast through winter

and causes, by spring, steeply sloping isohalines within the ACC, a weakly stratified water column and relatively high nearshore surface salinities (31–32) (Figure 2). In summer, relaxation of the downwelling winds and increased freshwater runoff diminishes nearshore salinities (29–31), enhances stratification, and spreads low-salinity waters offshore. Isohaline (and isopycnal) slopes decrease across the shelf, and at depths $> \sim 50$ m, there is an onshore transport of saline and nutrient-rich slope water [Childers et al., 2005; Weingartner et al., 2005]. Beginning in September/October, downwelling winds strengthen so that isohalines slope downward toward the coast, and the salinity in the ACC reaches its annual minimum (< 29) due to the seasonal accumulation of freshwater runoff (Figure 4). Low surface salinities (31–32) are now found across the shelf to at least the shelf break. The stratification, which is strongest over the shelf in July/August, decreases through October and rapidly diminishes by December. These changes, due to strengthening of the downwelling-favorable winds, result in steepening of the ACC’s isohalines and the formation of large horizontal salinity gradients over the inner shelf. Interannual salinity variations are largest (standard deviation $\sim \pm 2$) in July and October in the ACC within 40 km of the coast (inshore of GAK3) and in the upper 50 m. Elsewhere on the shelf and in other seasons, the standard deviation is $< \pm 0.4$. The effect of atmospheric heat transfer into and the vertical distribution of heat in the water column is therefore regulated by freshwater and salinity stratification [Janout et al., 2010].

[11] Minimum temperatures (5°C – 6°C) occur in spring when the shelf has a nearly uniform temperature distribution (Figure 3). However, nearshore waters are $\sim 3^\circ\text{C}$ during cold years [Janout et al., 2010]. Thermal stratification develops in summer, when temperatures can exceed 13°C in the upper 30 m (Figure 3). By October, surface waters cool to $< 11^\circ\text{C}$,

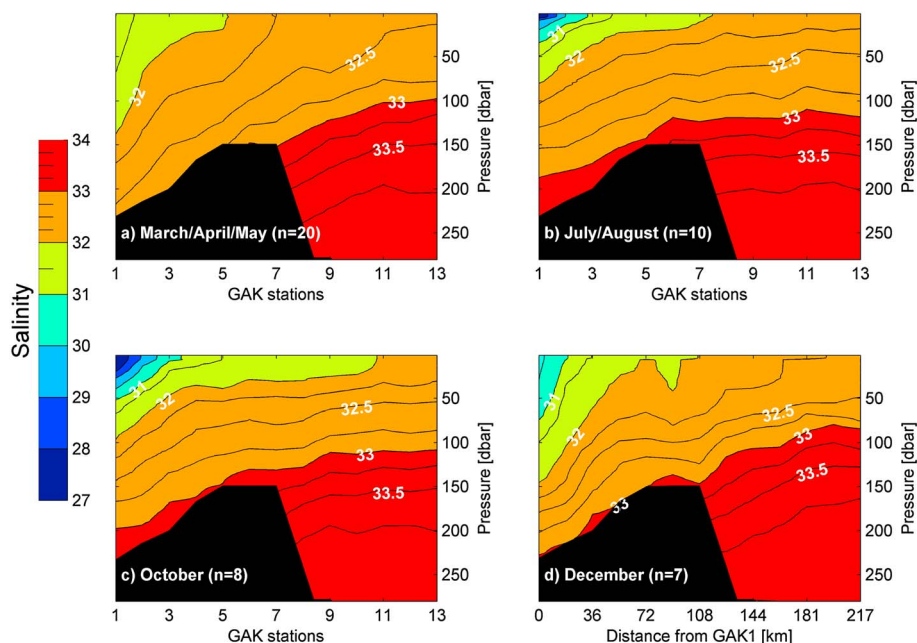


Figure 2. Seward Line salinity from GLOBEC cruises from 1997 to 2004, averaged for (a) March–May, (b) July–August, (c) October, and (d) December. The numbers of transects used for averaging are indicated by $n = 20$, $n = 10$, etc.

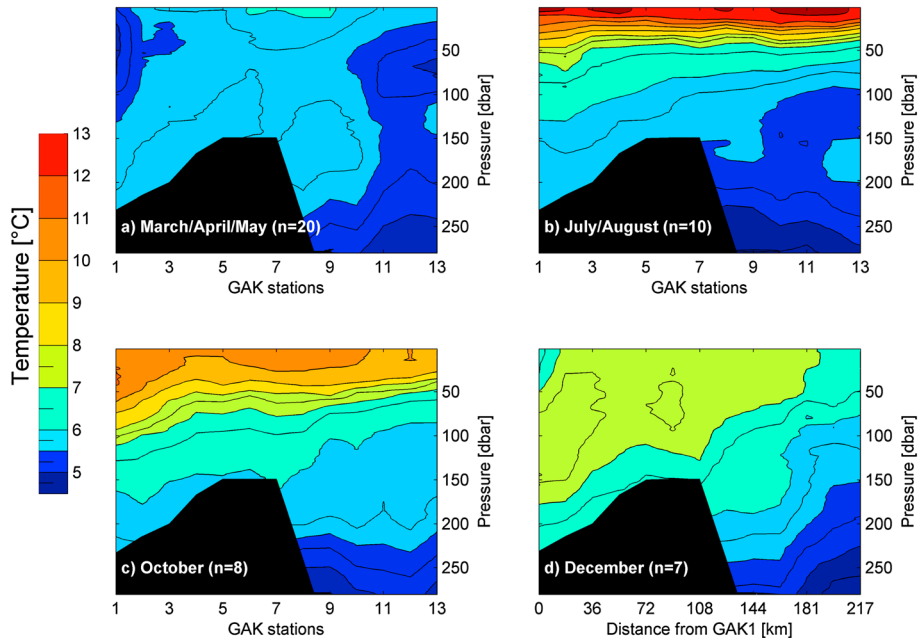


Figure 3. Seward Line temperature ($^{\circ}\text{C}$) from GLOBEC cruises from 1997 to 2004, averaged for (a) March–May, (b) July–August, (c) October, and (d) December. The numbers of transects used for averaging are indicated by $n=20$, $n=10$, etc.

and by December, temperatures are $<8^{\circ}\text{C}$ across the shelf. Temperature variability is largest near the surface (0–50 m) across the entire shelf in summer and fall with standard deviations of $\pm 2^{\circ}\text{C}$. Thermal stratification over the shelf is strongest in summer on the middle and outer shelves, offshore of the coastal freshwater influence, and in this season, it accounts for $\sim 75\%$ of the 0–50 m stratification. Cross-shelf temperature gradients are relatively weak throughout the year, with maximum temperature differences between the ACC and the outer shelf of $\sim 1^{\circ}\text{C}$ in October in the upper 50 m and with generally smaller differences ($<1^{\circ}\text{C}$) in deeper (>100 m) waters and in other seasons.

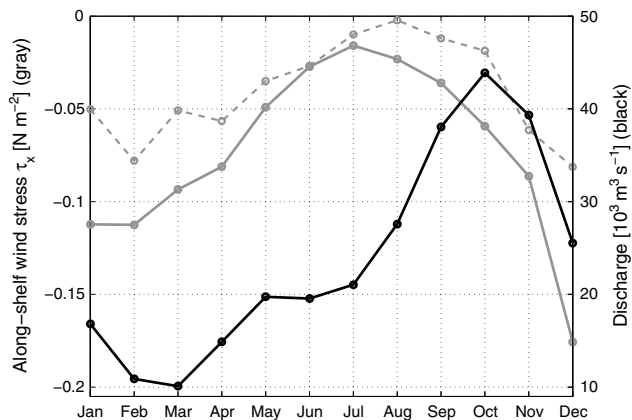


Figure 4. Climatology of coastal freshwater discharge (1932–2008, black) in south central and southeast Alaska from Royer’s [1982] hydrological model (right y axis) and QuikSCAT along-shelf wind stress [N m^{-2}] (2000–2008, gray, left y axis) at locations near GAK3 (solid gray) and GAK9 (dashed gray).

3.2. Air-Sea Fluxes and Oceanic Heat Content

[12] The seasonal net air-sea heat flux on the inner shelf (60°N , 146°W , Figure 1), based on the daily means (1948–2011) of NCEP latent and sensible heat fluxes and net long- and short-wave radiation, ranges from $<-250 \pm 250 \text{ W m}^{-2}$ in mid-winter to $\sim 150 \pm 50 \text{ W m}^{-2}$ in summer (Figure 5), where

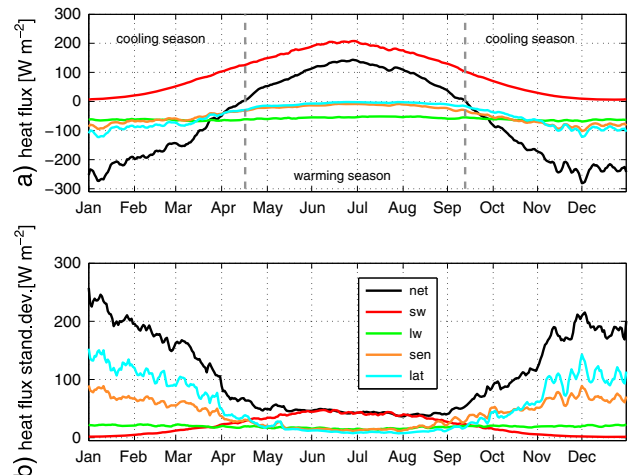


Figure 5. (top) Annual cycle of heat fluxes [W m^{-2}] at 60°N , 146°W , averaged from NCEP daily values from 1948 to 2011, and (bottom) their standard deviations. (black) Net air-sea fluxes, (red) short-wave radiation, (green) long-wave radiation, (orange) sensible fluxes, and (blue) latent fluxes. Negative fluxes denote heat transfer from ocean to atmosphere. Dashed gray lines indicate the transition into heating and cooling seasons based on the zero-crossings of the net heat flux. x-ticks mark the first day of each month. Data are smoothed with a 3 day running mean.

negative fluxes denote a heat transfer from ocean to atmosphere. The warming season begins on average on 15 April, while the average onset of the cooling season is 13 September. During the cooling season, the net heat flux is largely due to the latent and sensible heat fluxes, both having magnitudes of $\sim 100 \text{ W m}^{-2}$. However, the standard deviation in latent heat flux is nearly twice as large ($\pm 150 \text{ W m}^{-2}$) as that of sensible heat flux ($\pm 80 \text{ W m}^{-2}$). Long-wave radiation is approximately constant ($60 \pm 20 \text{ W m}^{-2}$) year-round. Short-wave radiation is negligible at the winter solstice but the largest contributor to the net air-sea heat flux in summer ($200 \pm 50 \text{ W m}^{-2}$). The net heat loss and gain offshore (58°N , 148°W , near GAK13) range from $-150 \pm 150 \text{ W m}^{-2}$ in winter to $+150 \pm 50 \text{ W m}^{-2}$ in summer and nearly balance one another on annual average. In contrast to that, the inner shelf has an annual mean deficit of 60 W m^{-2} , as indicated by both the long-term (1948–2011) and shorter-term (1997–2004) averaged NCEP air-sea heat fluxes. This deficit may in fact be larger ($\sim 80 \text{ W m}^{-2}$) if the bias in short-wave radiation of 20 W m^{-2} [Ladd and Bond, 2002] detected at Station Papa (50°N , 145°W) is applicable to the northern GOA as well. Thus, on annual average, the heat budget in the ACC must involve a net oceanic heat flux convergence in order to balance the air-sea heat flux deficit. Below, we estimate the along- and cross-shelf heat flux convergences needed to satisfy this deficit. The analysis is based on the estimates of the average monthly oceanic heat content (Q_{oc}) computed from the about seven annual Seward Line occupations between 1997 and 2004 for the ACC (GAK1-2) and the outer shelf (GAK7-8) (Figure 6) according to

$$Q_{oc} = \int_{\text{bottom}}^0 \rho c_p T dz$$

where ρ is the water density, $T(z)$ is the water temperature at depth z , and c_p is the specific heat of seawater, which ranges between 3980 and $4050 \text{ J kg}^{-1} \text{ K}^{-1}$ for GOA water properties [Fofonoff and Millard, 1983]. Oceanic heat content was computed for the entire water column. However, most of the seasonal hydrographic variability occurs above 150 m , the maximum mixed layer depth on the inner shelf [Sarkar et al., 2005]. The inner Seward Line is located in a particularly deep part of the shelf, whereas the maximum common depth along the Seward Line is 150 m , a bottom depth that is characteristic for much of the GOA shelf. This depth is also typically used for referencing velocities calculated from the thermal wind relation [Johnson et al., 1988], and the results are not sensitive to the integration depth. The middle shelf heat content (not shown) covaries with the outer shelf. Q_{oc} is at a minimum in March/April and maximum in October, with the largest amplitude on the inner shelf and smaller amplitudes on the middle and outer shelves. The local rate of change in oceanic heat content ($\partial Q_{oc}/\partial t$) is the net result of air-sea heat exchange and ocean heat flux convergence and also has a larger amplitude in the ACC than on the outer shelf. Over the outer shelf, $\partial Q_{oc}/\partial t$ varies from $\sim -80 \text{ W m}^{-2}$ in winter to $\sim +80 \text{ W m}^{-2}$ in summer, with these changes being nearly balanced by air-sea fluxes discussed above. In contrast, $\partial Q_{oc}/\partial t$ in the ACC varies from $\sim -130 \text{ W m}^{-2}$ in winter to nearly 120 W m^{-2} during summer (Figure 6). The oceanic heat flux convergence required to balance the ACC's heat budget is

thus $\sim 100 \text{ W m}^{-2}$ for the October–January average and $\sim 40\text{--}60 \text{ W m}^{-2}$ for the February–April (Figure 7) period, based on the difference between air-sea heat fluxes and the change in oceanic heat content. From June–August, the heat budget is nearly balanced. In the following section, we make rough estimates of the cross- and along-shelf heat fluxes and their contribution to the ACC (nearshore) heat budget.

3.3. Cross-Shelf Heat Transport

[13] Cross-shelf transport mechanisms on the northern GOA shelf include flow-topography interactions and eddy fluxes [Stabeno et al., 2004; Ladd et al., 2005], although these have not been quantified. In contrast to the importance of cross-shelf transport on the shelf's nutrient budget [Childers et al., 2005; Hermann et al., 2009], we expect that the net heat fluxes associated with these processes are

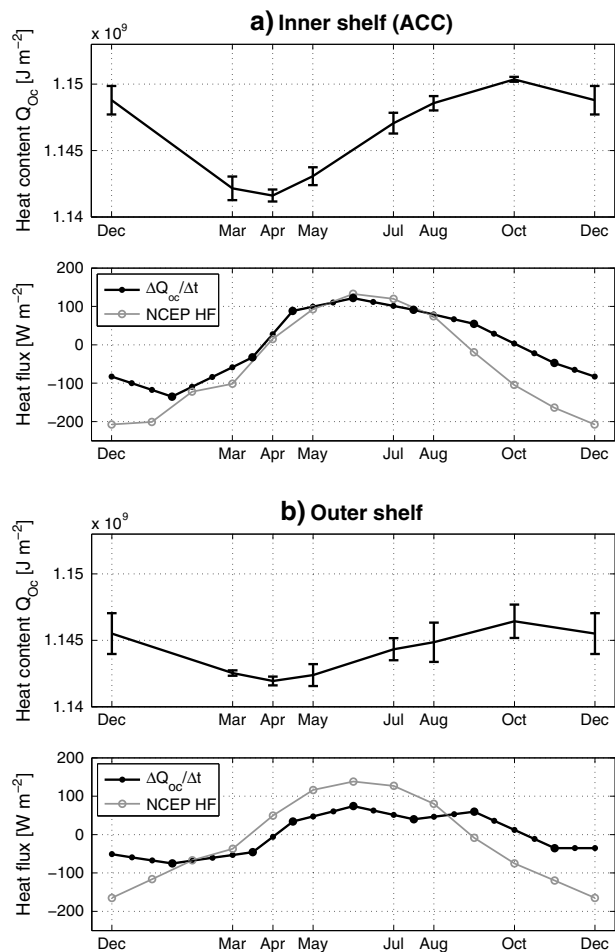


Figure 6. Seasonally averaged, depth-integrated (0 m bottom) oceanic heat content [Q_{oc}], including one standard deviation along the Seward Line for the (a) inner shelf (ACC) and (b) outer shelf. The companion panels show the temporal change in oceanic heat ($\Delta Q_{oc}/\Delta t$; black) and the monthly averaged NCEP net heat flux (gray). Note that Q_{oc} was interpolated from months with data coverage (large dots) to a biweekly time step (small dots) for computing the differences between air-sea fluxes and $\Delta Q_{oc}/\Delta t$ shown in Figure 7. Months labeled along the x axis indicate those months containing Seward Line data coverage. All values are based on 1997–2004 averages.

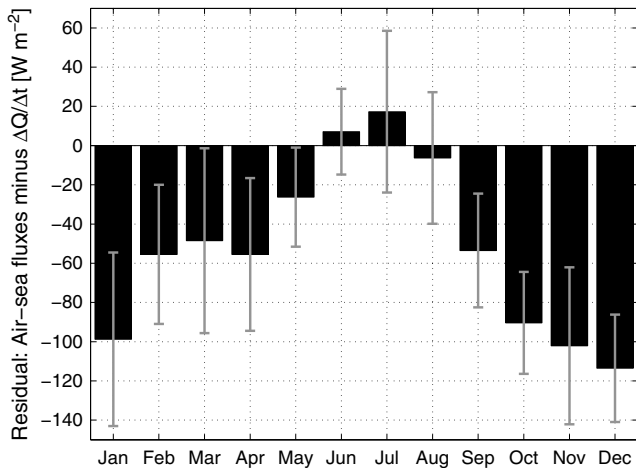


Figure 7. Nearshore (ACC) heat flux deficit between NCEP air-sea fluxes and the change in depth-integrated (surface–bottom) oceanic heat content at GAK1–2 shown in Figure 6a. The deficit indicates the amount of the ocean heat flux convergence required to balance the heat budget. Error bars show one standard deviation, indicating the inter-annual variability in the monthly differences.

negligible given the feeble cross-shelf temperature gradients and upon assuming that the mass-compensating onshore and offshore flows associated with these processes occur at approximately the same depth. Large anticyclonic slope eddies may impact the outer shelf’s heat and freshwater budgets [Janout *et al.*, 2009], but these occur irregularly and do not appear to influence the ACC; hence, they are also neglected. However, the prevailing downwelling-favorable winds from fall through spring impel a persistent Ekman transport that may influence the shelf heat budget.

[14] We thus take the net oceanic cross-shelf heat flux to be the result of difference in cross-shelf heat transport between the surface and bottom Ekman layers. Following Weingartner *et al.* [2005], we assume a two-dimensional mass balance in which the surface Ekman transport is balanced by a return flow that is (i) evenly distributed below the surface Ekman layer and (ii) entirely concentrated in a bottom Ekman layer. We used monthly mean zonal QuikSCAT wind stress τ_x from 2000 to 2008 and the Coriolis parameter f to compute monthly Ekman transport ($M_{\text{Ekman}}[\text{m}^2 \text{ s}^{-1}] = \tau_x / f$). The zonal wind stress is predominantly westward, and the onshelf Ekman transport is largest in late fall and early winter. Easterly winds weaken in summer (Figure 4) and, in some years, become weak westerly (upwelling-favorable). Hence, the total Ekman heat flux convergence is

$$HF_{\text{Ek}} = M_{\text{Ek}} \left(\frac{\partial Q_{\text{surf}}}{\partial y} - \frac{\partial Q_{\text{subsurf}}}{\partial y} \right).$$

Surface (0–20 m), subsurface (20 m to bottom), as well as near-bottom (230–250 m, not shown) cross-shelf heat gradients $\partial Q / \partial y$ [J m^{-4}] were computed from heat content differences between the outer (GAK7–8) and inner (GAK1–2) shelves (Figure 8) based on the average temperatures over these depths. The results are not sensitive to the choice of the Ekman layer thicknesses. As inferred from Figures 3 and 8, the heat content varies seasonally, but in general, the cross-shelf (meridional) heat gradients are negative from

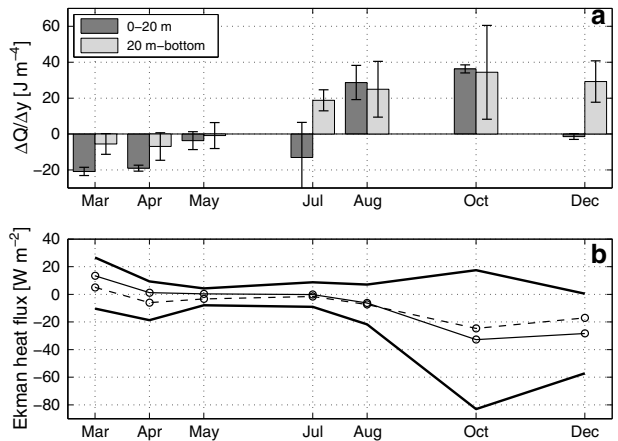


Figure 8. (a) Average oceanic cross-shelf (meridional) heat gradient [J m^{-4}] along the Seward Line for the surface (0–20 m, dark gray) and subsurface (20 m to bottom, light gray) layers. b) Cross-shelf ocean heat flux convergence [W m^{-2}] associated with Ekman transport. The dashed line is based on a subsurface return flow that is evenly distributed below the surface layer (dashed) or confined to the bottom boundary layer (solid). A negative heat flux indicates onshore heat transfer. The black lines outline a range using the bigger of the two standard deviations computed for each method for each month.

March through July, being $\sim -30 \text{ J m}^{-4}$ in the surface and smaller for subsurface depths. This gradient is positive and $\sim 15\text{--}30 \text{ J m}^{-4}$ in the surface and subsurface layers in August and October. Hence, for most of the year, the surface and subsurface cross-shelf heat gradients generally have the same sign. Exceptions occur in July and December, when these gradients are positive in subsurface waters and negative in the surface layer.

[15] The net cross-shelf Ekman heat flux convergence is thus onshore and a maximum ($\sim 20 \text{ W m}^{-2}$) in December and a minimum in summer of $< 3 \text{ W m}^{-2}$ (Figure 8). In October, the cross-shelf heat gradient is positive so that the net cross-shelf Ekman heat flux convergence tends to cool the inner shelf at $\sim 10 \text{ W m}^{-2}$. Although the standard deviation for Ekman heat flux convergence is small through most of the year ($< \pm 10 \text{ W m}^{-2}$), it is large in October and December ($\pm 20\text{--}30 \text{ W m}^{-2}$), which reflects the large variability in both winds and ACC temperatures mentioned in section 3.1. Although our computations suggest that Ekman transport may occasionally account for as much as 40 W m^{-2} (but generally $< 20 \text{ W m}^{-2}$), it is unclear if or how efficiently the onshore Ekman transport penetrates the ACC front. This front is strongest in fall when the onshelf Ekman heat flux convergence is largest. On an annual average, our estimate suggests that the net Ekman heat flux convergence makes a negligible ($\sim 5 \text{ W m}^{-2}$) contribution to the heat budget on the inner shelf of the GOA. Next, we will examine the contribution of along-shelf heat flux convergence.

3.4. Along-Shelf Heat Transport

[16] Flow over the middle and outer portions of the GOA shelf is weak and variable compared to the ACC [Stabeno *et al.*, 2004], and changes in oceanic heat appear to be approximately balanced by net air-sea fluxes in all seasons

(Figure 6). In contrast, the ACC has a large heat deficit from late fall through spring, which is not balanced by the cross-shelf Ekman heat flux convergence. Therefore, the bulk of the deficit must be balanced by the along-shelf advection of heat. This deficit (Figure 7) is on average $\sim 80 \text{ W m}^{-2}$ throughout the cooling season (October–April) and somewhat larger ($\sim 100 \text{ W m}^{-2}$) from October to January. The majority ($\sim 70\%$) of the baroclinic along-shelf transport on the northern GOA shelf is carried within the ACC [Weingartner *et al.*, 2005] with a mean annual transport of $\sim 0.8 \times 10^6 \text{ m}^3 \text{ s}^{-1}$ [Johnson *et al.*, 1988; Stabeno *et al.*, 1995]. Stabeno *et al.* [1995] estimated that the baroclinic component may amount to as much as 75% of the total ACC transport, depending on season and location, while Williams *et al.* [2007] estimate the baroclinic transport at 80%–90% under the strong downwelling winds characteristic of fall through early spring.

[17] From October to May, the 0–150 m averaged along-shelf heat gradients are $\sim 5.5 \pm 0.3 \text{ J m}^{-4}$ based on temperatures provided by the SODA ocean reanalysis (Figure 9). During winter, thermal stratification is weak, and the SODA temperatures indicate that the results are not sensitive to the layer thickness used to average the heat content to compute the gradients. The along-shelf heat gradients are largest ($6\text{--}8 \text{ J m}^{-4}$) in November and December, moderately strong from January through June ($4\text{--}6 \text{ J m}^{-4}$), and weakest from

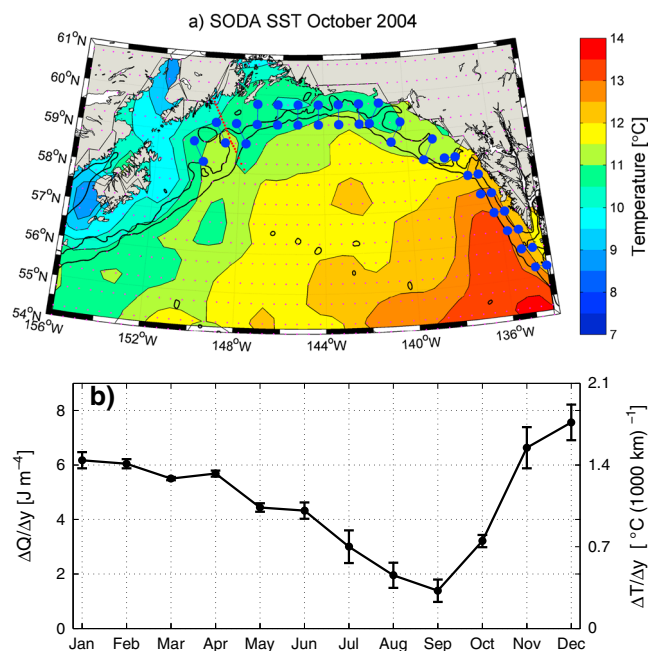


Figure 9. (a) Sea surface temperature [$^{\circ}\text{C}$] from the SODA ocean reanalysis for October 2004. Each pair of grid points (blue dots) was averaged and then used to calculate the along-shelf temperature/heat gradient. (b) Monthly means (1997–2004) of along-shelf heat and temperature gradients calculated from the grid points in Figure 9a. Error bars are based on the standard deviation from different results based on the layer thickness used to compute the average. A small standard deviation such as in March implies that similar gradients result from using the surface only to using a 0–150 m mean.

July through October ($1\text{--}3 \text{ J m}^{-4}$). We confine our estimates of along-shelf heat advection to the cooling season only, when the along-shelf thermal gradients are largest. We estimated the uncertainties in these gradients by varying the averaging depth between the surface and 150 m in $\sim 10 \text{ m}$ increments. The SODA gradients are similar in magnitude to our estimates of $\sim 4 \pm 1 \text{ J m}^{-4}$ based on sea surface temperature differences between National Data Buoy Center (NDBC) buoys 60082 and 60084, between different NCEP grid points and from conductivity-temperature-depth (CTD) profiles at Cape Suckling (see Figure 1 for locations) and the Seward Line in December 1999, and from the moored temperature records.

[18] The October–January ACC heat budget deficit of 100 W m^{-2} implies that westward current speeds must be $\sim 0.08\text{--}0.22 \text{ m s}^{-1}$, for values of $\partial Q_{oc}/\partial x$ ranging between 3 and 8 J m^{-4} . This estimate is consistent with other, albeit limited, measurements. For example, Johnson *et al.* [1988] report depth-averaged, along-shelf westward currents for December 1983 of 0.2 m s^{-1} from moored current meter records. We also estimate the along-shelf geostrophic velocities for the 1997–2004 period from the thermal wind relation applied to stations along the Seward Line, assuming a level of no motion at 150 m. We estimated these for each cruise and computed the monthly means (Figure 10). Over the outer shelf, along-shelf velocities vary from -0.06 m s^{-1} in December and May to $\sim 0 \text{ m s}^{-1}$ in July. Within the ACC, the thermal wind relation indicates that depth-averaged, along-shelf velocities range from -0.05 m s^{-1} in July to -0.18 m s^{-1} in December, with these variations consistent with the seasonal cycles of wind and runoff (Figure 4).

[19] For comparison, we computed monthly and seasonal averages from the velocity records obtained in 2001/2002 and 2002/2003 from the moorings on the inner Seward Line and from those offshore of Gore Point (Figure 1). The October–December (20–100 m) mean flow in the ACC estimated from three current meters from the inner Seward Line was 0.17 m s^{-1} , while the mean flow in the ACC near Gore Point was similar (0.19 m s^{-1}). These averages are

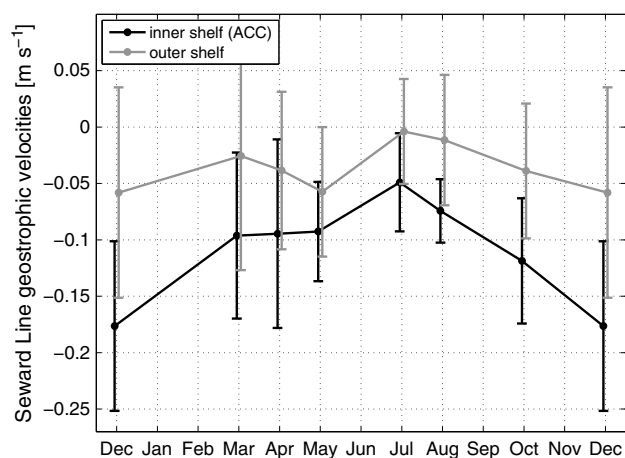


Figure 10. Mean (0–150 m) along-shelf geostrophic velocities [m s^{-1}] computed from 1997 to 2004 Seward Line CTD data from inner (GAK1–2, black) and outer (GAK7–8, gray) shelf stations. Error bars indicated one standard deviation.

15%–27% higher than those estimated using the thermal wind relation. The February–April means at both mooring locations are 0.10 and 0.15 m s^{-1} , i.e., 12%–62% higher than those derived from the thermal wind, which may be expected since the barotropic velocity component increases the flow magnitude measured by the moorings. The mooring records used for these estimates are from winters with slightly below (2001/2002) and above (2002/2003) average coastal runoff and winds [Janout *et al.*, 2010], and they likely bracket the average current velocities for these months.

3.5. Cross- and Along-Shelf Air-Sea Heat Flux Variability

[20] The previous sections highlighted considerable cross-shelf gradients in along-shelf baroclinic transport (Figure 10), oceanic heat content (Figure 6), and along-shelf wind stress (Figure 4). This spatial variability may have significant consequences on air-sea fluxes and the oceanic heat budget across the shelf. For a northern GOA-wide comparison of air-sea fluxes, we searched the NDBC data base for weather buoys with simultaneous data coverage and computed turbulent (latent and sensible) heat fluxes. Turbulent fluxes compose the largest part of the air-sea winter heat flux (Figure 5) and are also the largest source of variability in these fluxes. Although the bulk of the winter cooling occurs from November through March, this part of our analysis is constrained to the 4 month period between January and April for the years 2003, 2004, 2006, and 2008 due to limited concurrent buoy data. We then combine single buoys into regional averages and compute the cumulative sum of the fluxes in order to describe spatial heat flux variations over the northern GOA shelf (Figure 11a). The results indicate that winter air-sea heat fluxes increase from offshore to onshore and from east to west around the GOA, as additionally supported by winter-averaged NARR fluxes (Figure 11b). For example, the cumulative turbulent heat fluxes in Shelikof Strait are more than twice those over the basin southeast of Kodiak Island. Heat fluxes in Prince William Sound (PWS) are $\sim 20\%$ less than those in Shelikof Strait, but $\sim 15\%$ greater than Cape Suckling and Southeast Alaska and 30% larger than for Middleton Island (PAMD) on the outer shelf, which is only ~ 90 km south of PWS. The average January–April air temperature of the PWS buoys is only $\sim 0.4^\circ\text{C}$ lower than at PAMD during the 4 years used to construct Figure 11a, and therefore, the cross-shelf heat flux gradients between the outer and inner shelves and PWS are largely due to cross-shelf wind gradients as discussed next.

[21] Zonal means of the 2000–2008 monthly QuikSCAT and NARR wind speeds between 140°W and 150°W (roughly between Yakutat and GAK1, see Figure 1) on the northern GOA shelf show that wind speeds ~ 80 km offshore of the coast are 30% – 35% smaller than those adjacent to the coast (Figure 12). Cross-shelf wind speed gradients diminish in spring and are slightly reversed in summer. Figure 13 shows how the ratio of the inner to outer shelf wind speeds, averaged over the November–March period, varies along-shelf in this region. Ratios greater than 1.2 are found at $\sim 146^\circ\text{W}$ in eastern PWS, between 143°W and 146°W near the Copper River delta and the Cordova-Valdez mountains, the western entrance to PWS (148°W), and the mouth

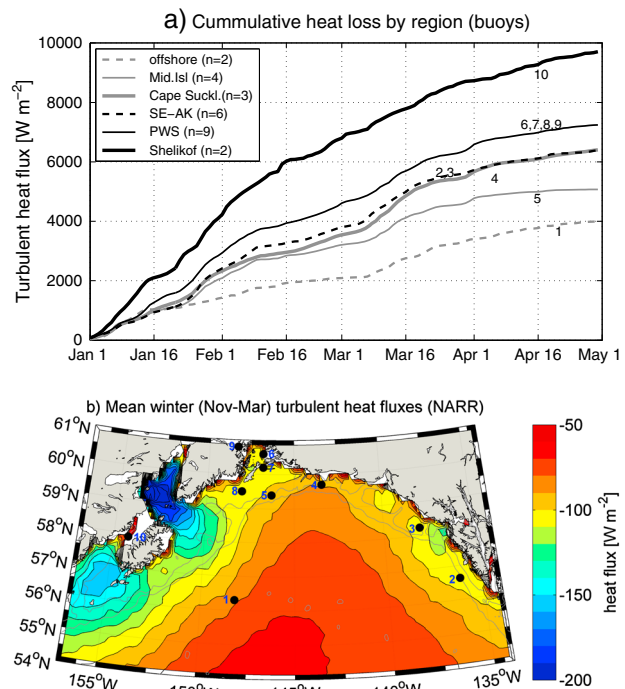


Figure 11. (a) Average January–April cumulative turbulent heat loss in the GOA, computed from weather buoys from selected locations (see map in Figure 1). Mean values were composed from available buoys among 2003, 2004, 2006, and 2008. Number of data points used for the mean is shown in legend ($n=2$, etc.). Numbers on the graphs correspond to the buoy number in Figure 1 used to construct the graphs. (b) Mean winter (November–March) latent + sensible heat flux from NARR [W m^{-2}], including locations of the weather buoys used to construct Figure 11a.

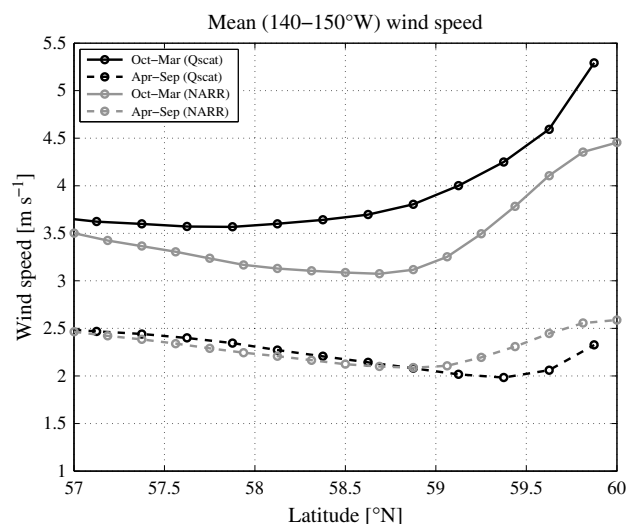


Figure 12. Zonally averaged QuikSCAT wind speeds [m s^{-1}] between 140°W and 150°W for (black solid) October–March and (black dashed) April–September compared with the corresponding NARR wind speeds in gray. Standard deviations (not shown) decrease seaward and are maximum inshore in October–December ($\pm 1.1 \text{ m s}^{-1}$), except April–June, when the standard deviation is larger offshore ($\pm 0.9 \text{ m s}^{-1}$) than nearshore ($\pm 0.6 \text{ m s}^{-1}$).

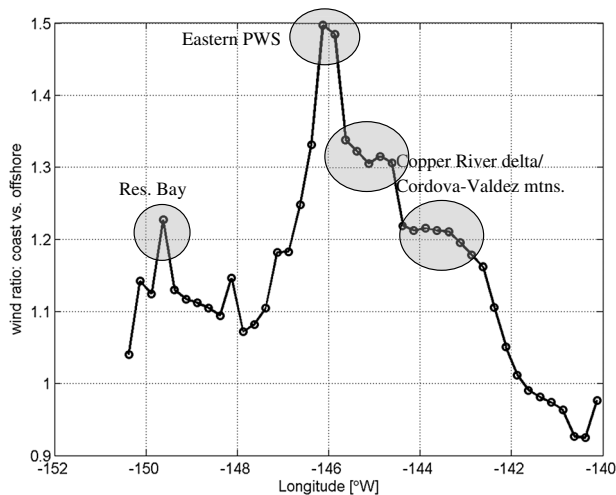


Figure 13. Meridional (November–March, 2000–2008) average of the QuikSCAT wind speed ratio nearshore to ~ 80 km (0.75° latitude) seaward of the nearshore data point. Gray shades highlight peaks in the ratio as described in the text.

of Resurrection Bay ($\sim 149^\circ$ W). These are areas where barrier jets and gap winds occur during the cooling season [Macklin *et al.*, 1988; Loescher *et al.*, 2006]. Barrier jets blow along the coast and are generated during onshore air-flow, while (seaward-oriented) gap winds are channeled through gaps in the coastal topography [Loescher *et al.*, 2006]. Both are intimately linked to the mountainous coastline [Macklin *et al.*, 1988; Overland and Bond, 1993]. Loescher *et al.* [2006] found that $>80\%$ of all barrier and hybrid (combination of barrier and gap wind) jets are <80 km wide. Their result agrees with Macklin *et al.* [1988], who showed that these ageostrophic nearshore wind events adjust geotriply within one Rossby radius of deformation (~ 60 km) from shore. Their findings are also consistent with the large cross-shelf gradients observed in the QuikSCAT and NARR wind speeds (Figure 12) and the large differences in air-sea heat fluxes between PWS and Middleton Island (PAMD). Although PAMD is only 90 km south of PWS, it is beyond the influence of these mesoscale wind phenomena. The impact of these nearshore wind events on cooling of the ACC is therefore substantial. This may be especially so since a substantial portion of the ACC appears to flow through PWS [Niebauer *et al.*, 1994].

[22] The Shelikof Strait buoy indicates considerably higher oceanic heat loss in this region than elsewhere on the shelf. In winter, this strait is apparently dominated by strong low-level wind jets that are controlled by the channel’s topography [Lackmann and Overland, 1989; Macklin *et al.*, 1990; Liu *et al.*, 2006]. These jets extend over a broader area that includes Cook Inlet and the shelf north of Kodiak Island as evidenced by the NARR heat flux patterns in the northwestern GOA. This cooling is reflected in the depth-averaged temperature data from May CTD casts, which suggest that average temperatures can be 1°C – 2°C lower in Shelikof Strait than at GAK1 [Stabeno *et al.*, 2004]. Hence, the along-shelf temperature gradient between GAK1 and Shelikof Strait is $\sim -3^\circ\text{C}$ (1000 km) $^{-1}$ or nearly

twice the estimated $\sim -1.5^\circ\text{C}$ (1000 km) $^{-1}$ temperature gradient to the east of GAK1. In the next section, we investigate the sea level pressure (SLP) distributions over the northern GOA that give rise to these spatial variations in wintertime air-sea heat fluxes.

3.6. The Role of Northern GOA Low Sea Level Pressure Events

[23] A more detailed examination of the January–April turbulent fluxes discussed above indicated that each of the 4 years used to construct Figure 11a included a number of vigorous cooling events, where the heat loss exceeded the winter-averaged heat loss by 50%–100%, with each event lasting from 2 to 10 days. The aggregate heat loss during these short-term events amounts to $\sim 40\%$ – 60% of the total January–April heat loss. Inspection of the SLP distributions (not shown) shows that each cooling event is generally associated with a low-pressure system located in the northern GOA. The influence of GOA lows on the North Pacific’s oceanic and atmospheric conditions are well known [Overland and Hiester, 1980; Rodionov *et al.*, 2007; Janout *et al.*, 2010], and we here show that the propagation and residence time of northern GOA lows is a major factor in the spatiotemporal variability of northern GOA heat fluxes.

[24] Overland and Hiester [1980] applied correlation techniques to analyze northern GOA sea level pressure data for dominant weather systems, which allowed them to categorize and quantify the occurrence of specific weather patterns during 1968–1977. We followed a similar, but simpler approach, in quantifying the occurrence of low-pressure systems in the northern GOA during winter (November–March). Overland and Hiester [1980] defined six different weather patterns in this region, but we specifically concentrate on SLP patterns with minimum pressure in the northern GOA. Specifically, we screened six hourly (1948–2012) NCEP SLP within 130°W – 180°W and 50°N – 62.5°N and enumerated occasions where a minimum SLP was found within the region bounded by 57.5°N – 62.5°N , and 130°W – 155°W . The time during which a low was found in the northern GOA divided by the total time period considered provides an index for the frequency of occurrence (F_o) of northern GOA low-pressure systems, i.e.,

$$F_o = 100 \times \frac{\text{time}_{\text{GOA low}}}{\text{time}_{\text{total}}} [\%].$$

The mean November–March anomalies of F_o and air temperatures (Figure 14) from a northern GOA NCEP grid point (60°N , 146.5°W) (Figure 1) are significantly anticorrelated ($r = -0.53$, $p < 0.01$). The 1948–2012 November–March average F_o is $\sim 18\%$, while the 1968–1977 average is 21% and only slightly higher than Overland and Hiester’s [1980] 1968–1977 winter average of 16%. The maximum F_o of $\sim 28\%$ occurred in 2012, which was slightly larger than 1971 (26%), 1972 (26%), 1975 (27%), and 2007 ($\sim 25\%$). The minimum F_o of $\sim 9\%$ occurred in 2003. The 1976/1977 regime shift [Mantua *et al.*, 1997] is evident in the F_o time series as high (low) F_o and low (high) air temperatures were more common during the period before (after) the regime shift. Moreover, the early 1970s and 2007 and 2008 are consistent with periods of anomalously low northern GOA shelf temperatures [Janout *et al.*, 2010].

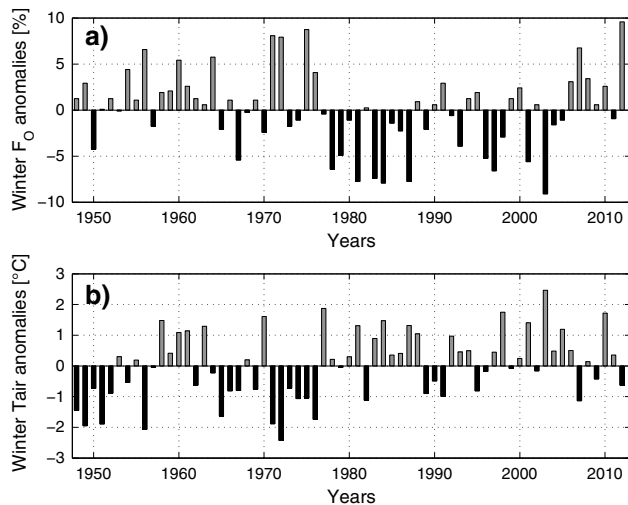


Figure 14. Anomalies of (top) the November–March averages of frequency of occurrence (F_o) of lows in the northern ($\geq 57.5^\circ\text{N}$ $\leq 62.5^\circ\text{N}$) GOA and (bottom) NCEP air temperatures [$^\circ\text{C}$] from 1948 to 2012 at 60°N , 150°W . These two time series are significantly anticorrelated ($r = -0.53$, $p < 0.01$). Gray (black) bars indicate positive (negative) anomalies.

The occurrence and duration of low SLP systems that propagate into the northern GOA account for $\sim 28\%$ of the interannual variability in northern GOA air-sea heat fluxes.

[25] The position of the lows also explains the along- and cross-shelf variations in the heat fluxes. NCEP air temperature anomalies and SLP from March 2007 (as an example of an anomalously cold month in the northern GOA) indicate that low pressure centered at the head of the GOA causes below normal air temperatures primarily along the western flank of the low because northerly winds bring cold continental air southward from Alaska’s interior (Figure 15). In contrast, the eastern GOA (between 50°N and 57°N) shows near-average air temperatures due to eastward (i.e., shoreward) advection of oceanic air masses. Furthermore, lows tend to concentrate along the north central portion of the GOA basin, because the coastal mountains impede inland propagation [Wilson and Overland, 1986]. For example, lows are centered between 140°W and 150°W $\sim 50\%$ of the time, while east of 140°W they occur only 23% of the time. We next compare winter heat fluxes and their anomalies at three NCEP grid points at nearshore locations in the eastern, central (south of PWS), and northwestern GOA (east of Kodiak) (Figure 1) from 1948 to 2012 and thereby distinguish between average winter (November–March) heat flux (Figure 16a) and the average winter heat flux during the occurrence of northern GOA lows (Figure 16b). In addition, we computed the winter heat flux anomalies (Figure 16c) and compare these with those heat flux anomalies associated with the presence of northern GOA lows (Figure 16d). On winter average, the northeastern GOA has relatively moderate mean winter heat fluxes of $-140 (\pm 35) \text{ W m}^{-2}$, while mean heat fluxes are $-155 (\pm 40) \text{ W m}^{-2}$ in the north central GOA and $-190 (\pm 45) \text{ W m}^{-2}$ in the northwestern GOA.

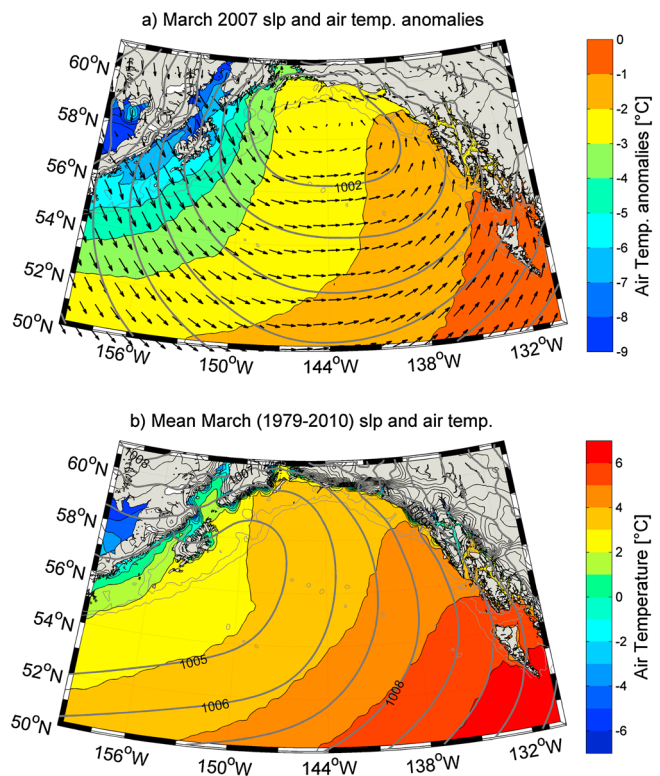


Figure 15. a) March 2007 NARR monthly mean sea level pressure (SLP, contours), air temperature anomalies [$^\circ\text{C}$] (color), and wind speed (arrows) based on the March 1979–2010 period. SLP [mbar] contours are in 2 mbar increments. (b) Mean 1979–2010 March air temperatures [$^\circ\text{C}$] (color) and SLP [mbar] (contours).

[26] The winter heat fluxes and their anomalies (Figures 16a and 16c) are spatially coherent and show a uniform shift from negative to positive anomalies during the 1977 regime shift [Mantua et al., 1997] at each of the three locations. Interestingly, when averaging winter heat fluxes exclusively during the occurrence of northern GOA lows, the three grid points show significant differences (Figure 16b). Under these conditions, the eastern GOA has an average heat loss of $-120 \pm 30 \text{ W m}^{-2}$, with positive anomalies of $+20 \pm 25 \text{ W m}^{-2}$ (Figure 16d), while the north central GOA loses more heat ($-190 \pm 55 \text{ W m}^{-2}$), with negative anomalies of $-30 \pm 50 \text{ W m}^{-2}$. However, for the northwestern GOA, heat fluxes are $-380 \pm 100 \text{ W m}^{-2}$, with the largest anomalies of $\sim -190 \pm 95 \text{ W m}^{-2}$. This implies that winter northern GOA lows reduce cooling rates in the eastern GOA but enhance cooling in the north central and northwest GOA. Drifter observations made during fall indicate that it takes from 1 to 3 months for water parcels to transit the $\sim 800 \text{ km}$ distance from Cook Inlet to Unimak Pass [Stabeno et al., 2002; Janout et al., 2009]. Hence, as the ACC flows through this region in winter, it is subjected to substantially greater cooling than elsewhere on the shelf. The results also imply that low-pressure systems centered over the northern GOA impact the heat budget of the south-east Bering Sea shelf both directly through air-sea heat fluxes over that shelf and indirectly through strong cooling of GOA shelf waters that ultimately enter the Bering Sea.

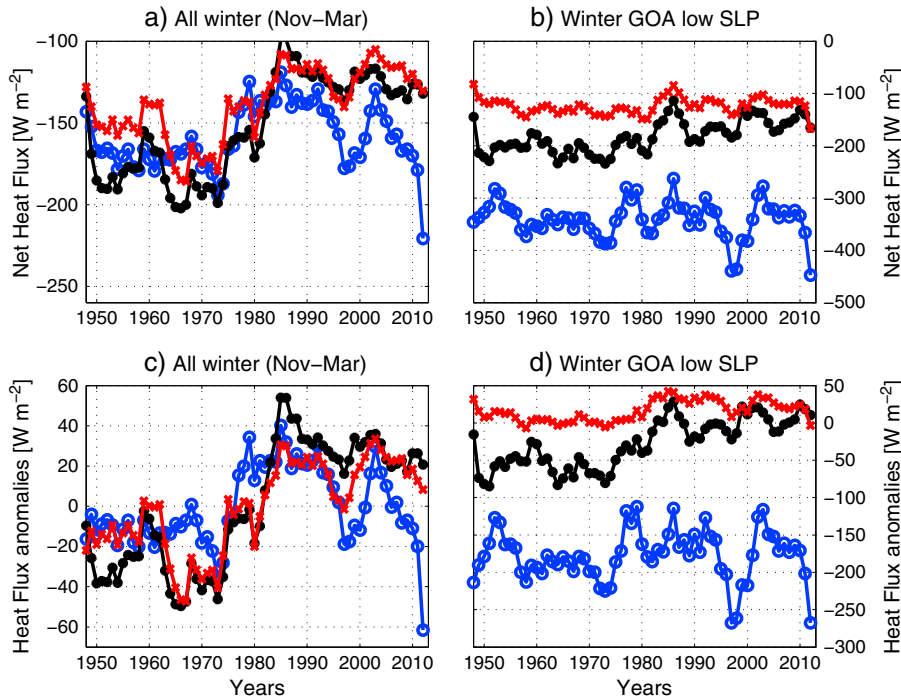


Figure 16. (a, b) Net air-sea fluxes [W m^{-2}] and (c, d) their anomalies from three locations around the northern GOA (red: SE-AK; black: SC-AK; blue: Western-AK. See locations in Figure 1). The plot shows one data point for each winter with a three-point running mean applied. Note that the plots include the last two data points to include the extreme anomaly in winter 2012. Data were averaged from six hourly NCEP fluxes from 1948 to 2012. Figures 16a and 16c are from net winter (November–March) air-sea fluxes. Figures 16b and 16d include only the data between November and March during the occurrence of a low-pressure system in the northern GOA, i.e., from data points used for the frequency of occurrence (F_o) computations in Figure 14.

4. Summary and Discussion

[27] We presented climatological estimates of air-sea heat fluxes and oceanic along- and cross-shelf heat advection and their relative contributions to the northern Gulf of Alaska (GOA) oceanic heat budget computed from averaged Seward Line observations from 1997 to 2004. The data set is limited, and thus, our oceanic heat flux convergence estimates are coarse and should be regarded as tentative. Notwithstanding these limitations, the results suggest that the oceanic processes affecting the heat budget on the northern GOA shelf vary seasonally. Over the outer shelf, the heat budget appears to be balanced by air-sea heat exchanges throughout the year. Within the Alaska Coastal Current (ACC; inner shelf), the summer heat budget is primarily controlled by air-sea heat exchange. From fall through late winter, the inner shelf cools due to heat loss to the atmosphere. This heat loss is partially buffered by along-shelf heat flux convergences, which are a maximum of $\sim 100 \text{ W m}^{-2}$ in fall and diminish to $\sim 40 \text{ W m}^{-2}$ in spring (Figure 7). By comparison, the net air-sea heat fluxes average ~ -200 and $\sim -100 \text{ W m}^{-2}$ between early and late winter, respectively. The along-shelf heat flux convergences within the ACC offset the heat loss to the atmosphere by $\sim 50\%$ in early and $\sim 10\%$ in late winter/spring.

[28] The cross-shelf heat flux convergence estimates are based solely on fluxes associated with net cross-shelf Ekman

transports and do not include heat fluxes associated with eddies and/or advective heat fluxes mediated by topographically steered currents over the complex bathymetry of the GOA shelf. On average, cross-shelf heat flux convergence appears to be weak ($\sim 5 \text{ W m}^{-2}$ on annual average). These fluxes tend to cool the inner shelf in fall, but heat it in late winter/spring. The variability in the Ekman-induced cross-shelf heat flux convergence is much larger than the mean in fall and early winter, suggesting that these fluxes may be an important source of interannual variability. Given the limitations in our observations-based analysis, a profitable direction for future research is to investigate the seasonally (and interannually) varying heat budget of this shelf using high-resolution numerical models.

[29] The fall–winter reversal in the sign of the cross-shelf heat flux is due to a reversal in the sign of the cross-shelf temperature gradients and not changes in wind direction, which are downwelling-favorable from fall through spring (Figure 4). The seasonal changes in the sign of the cross-shelf temperature gradients arise due to greater air-sea heat exchange over the inner shelf compared to offshore. The cross-shelf gradient in atmospheric cooling is associated with the coastal mountains, which result in colder (and drier) air temperatures nearshore compared to offshore and orographic inducement of ageostrophic barrier jets and gap winds [Loescher *et al.*, 2006; Macklin *et al.*, 1988] that are generally confined to within $\sim 70 \text{ km}$ of the coast.

[30] There are also large along-shelf gradients in winter air-sea heat loss, with these gradients dependent upon the position of the Aleutian Low in winter. In the mean, the Low is centered in the western GOA between 56°N and 58°N (Figure 15) so that average winter air temperatures decrease and air-sea heat losses increase, moving counterclockwise around the GOA shelf. However, much of the interannual variability in winter cooling is associated with the position of the Aleutian Low. The lowest spring ocean temperatures on record occurred in years when the frequency of occurrence (F_o) of northern GOA lows was greatest. (We defined northern GOA lows as those having centers between 57.5°N and 62.5°N and 130°W and 155°W). “Northern” lows tend to be weaker but centered farther north than average. They affect ocean cooling in two ways. First, these systems result in larger air-sea heat losses than average, especially over the western side of the low, thereby intensifying the east–west contrast in air-sea cooling over the GOA. Second, the along-shelf baroclinic transport within the ACC is reduced in these cases, which undermines the heat buffering tendency associated with winter along-shelf heat flux convergence. That reduction evolves because of decreases in both downwelling-favorable wind stress and winter coastal discharge [Janout et al., 2010]. Discharge also affects wintertime stratification over the inner shelf, so that the spring temperature distribution over the shelf is intimately connected to the winter hydrologic regime.

[31] Our findings show that the nearshore GOA has an annually averaged surface heat flux deficit, which is balanced by along-shelf heat flux convergence in winter. This contrasts with some midlatitude shelves, which, often characterized by a surplus in surface heat fluxes, require ocean heat flux divergence as a source of cooling. For instance, Lentz [2010] estimated that the Middle Atlantic Bight’s long-term averaged surface heat flux surplus ($\sim 10 \text{ W m}^{-2}$) is primarily balanced by cold southward (along-shelf) currents. On the outer New England shelf, Lentz et al. [2010] showed that surface fluxes in summer are balanced by cross-shelf heat removal, while in winter, along-shelf advection imposes strong cooling on the region’s waters. The low summer temperatures on the shallow inner New England shelf result from a balance between surface fluxes and the cross-shelf advection (upwelling) of cold water, whereas the winter heat budget is a function of surface fluxes only [Fewings and Lentz, 2011]. For the North Carolina shelf, Austin [1999] found that the summer heat content is dominated by cross-shelf fluxes, while along-shelf heat advection dominates during winter. Furthermore, on upwelling-dominated shelves, a surface heat surplus is to first order balanced by Ekman offshore heat transport, as shown on the northwest African shelf during spring [Richman and Badan-Dangon, 1983] as well as the northern California shelf, where the heat budget during the spring and summer upwelling season is essentially two dimensional [Lentz, 1987; Rudnick and Davis, 1988], while it becomes three dimensional in winter due to a decreasing cross-shelf circulation and an increase in the relative importance of along-shelf advection [Dever and Lentz, 1994]. The importance of cooling by along-shelf advection increases further offshore in the California Current system [Bograd et al., 2001; Edwards and Kelly, 2007]. Overall, a major contrast between the GOA and these midlatitude shelves is

noticeable in the opposite role of ocean advection in balancing the heat budget, which in the GOA is primarily achieved by the along-shelf heat flux convergence in the ACC.

[32] The GOA shelf represents one component of the large-scale shelf circulation that carries Pacific waters northward and eventually into the Arctic Ocean [Aagaard et al., 2006]. It appears that the ACC is an important source of freshwater [Weingartner et al., 2005; Aagaard et al., 2006] and possibly heat [Stabeno et al., 2005] for the Bering Sea shelf. With respect to the Bering Sea shelf’s heat budget, we note that years in which the F_o of northern GOA lows is anomalously large coincide with an extensive winter ice cover and summer “cold pool” on the Bering Sea shelf [Grebmeier et al., 2006; Rodionov et al., 2007; Danielson et al., 2011]. Although the processes leading to these conditions are largely endemic to the Bering Sea shelf, our results imply that the heat flux contribution from the GOA to the Bering Sea shelf is also reduced in such years, due to both a reduction in the baroclinic flow and a reduction in the transport through Unimak Pass during westerly wind anomalies [Stabeno et al., 2002], thus aggravating cooling over the Bering Sea. Over much of the Bering Sea shelf, oceanic-heat flux convergence is weak and largely controlled by winds [Reed and Stabeno, 2002; Danielson et al., 2011]. However, over the northern Bering Sea and in Bering Strait, the along-shelf (northward) transport of heat significantly contributes to the shelf heat budget through summer and fall [Woodgate et al., 2010]. Within the Chukchi Sea, the northward advective heat flux plays an important role in summer sea ice retreat [Weingartner et al., 2005; Woodgate et al., 2005; Spall, 2007]. By fall, along-shelf heat advection exceeds air-sea cooling and is thus instrumental in delaying the onset of ice formation on this shelf [Weingartner et al., 2013].

[33] Our analysis has enabled only coarse estimates of some of the components of the seasonally varying heat budget of the northern GOA shelf. The heat budget’s seasonal and interannual variability is primarily governed by the strength and position of the Aleutian Low. These parameters affect spatial patterns and magnitudes of air-sea heat exchanges and, via winds and precipitation, the stratification and the circulation of this shelf. These effects are, to some extent, propagated into the Bering Sea and thus influence that ecosystem as well.

[34] **Acknowledgments.** Hydrographic sampling along the Seward Line from 1998 to 2004 was carried out as part of NEP-GLOBEC and since 2005 under support of the NPRB (Projects 520, 603, 708, and 804). NCEP Reanalysis data were provided by the NOAA-CIRES Climate Diagnostics Center, Boulder, CO, USA, from their Web site at <http://www.cdc.noaa.gov/>. QuikSCAT data are produced by Remote Sensing Systems and sponsored by the NASA Ocean Vector Winds Science Team. Data are available at <http://www.remss.com>. Buoy data were downloaded from the National Data Buoy Center (NDBC) website at <http://www.ndbc.noaa.gov/> and from the Alaska Ocean Observing System at <http://www.aos.org/>. The SODA data were obtained from <http://www.atmos.umd.edu/~ocean/data.html>. Hydrographic sampling at GAK 1, the GAK 1 mooring, and support for TW are provided by the Exxon Valdez Oil Spill Trustees Council. We thank Dave Kachel for providing the mooring data and Seth Danielson for help with NARR data. We greatly appreciate the comments from two anonymous reviewers, which significantly improved the manuscript.

References

Aagaard, K., T. J. Weingartner, S. L. Danielson, R. A. Woodgate, G. C. Johnson, and T. E. Whitledge (2006), Some controls on flow

- and salinity in Bering Strait, *Geophys. Res. Lett.*, *33*, L19602, doi:10.1029/2006GL026612.
- Anderson, P. J., and J. F. Piatt (1999), Community reorganization in the Gulf of Alaska following ocean climate regime shift, *Mar. Ecol. Prog. Ser.*, *189*, 117–123.
- Austin, J. A. (1999), The role of the alongshore wind stress in the heat budget of the North Carolina inner shelf, *J. Geophys. Res.*, *104*(C8), 18,187–18,204.
- Bograd, S. J., T. K. Chereskin, and D. Roemmich (2001), Transport of mass, heat, salt, and nutrients in the southern California Current System: Annual cycle and interannual variability, *J. Geophys. Res.*, *106*, 9255–9275.
- Carton, J. A., and B. S. Giese (2008), A reanalysis of ocean climate using Simple Ocean Data Assimilation (SODA), *Mon. Weather Rev.*, *136*, 2999–3017.
- Childers, A. R., T. E. Whitledge, and D. A. Stockwell (2005), Seasonal and interannual variability in the distribution of nutrients and chlorophyll-a across the Gulf of Alaska shelf: 1998–2000, *Deep Sea Res., Part II*, *52*, 193–216.
- Coyle, K. O., Eisner, L., Mueter, F., Pinchuk, A., Janout, M., Cieciel, K., Farley, E., et al. 2011. Climate change in the southeastern Bering Sea: Impacts on Pollock stocks and implications for the Oscillating Control Hypothesis, *Fish. Oceanogr.*, *20*, 139–156.
- Danielson, S., L. Eisner, T. Weingartner, and K. Aagaard (2011), Thermal and haline variability over the central eastern Bering Sea shelf: seasonal and interannual perspectives, *Cont. Shelf Res.*, *31*:539–554.
- Dever, E. P., and S. J. Lentz (1994), Heat and salt balances over the northern California shelf in winter and spring, *J. Geophys. Res.*, *99*(C8), 16,001–16,017.
- Edwards, K. A., and K. A. Kelly (2007), A seasonal heat budget across the extent of the California Current, *J. Phys. Oceanogr.*, *37*, 518–530.
- Fairall, C. W., E. F. Bradley, D. P. Rogers, J. B. Edson, and G. S. Young (1996), Bulk parameterization of air-sea fluxes for Tropical Ocean Global Atmosphere Coupled Ocean Response Experiment, *J. Geophys. Res.*, *101*, 3747–3764.
- Fairall, C. W., E. F. Bradley, J. E. Hare, A. A. Grachev, and J. B. Edson (2003), Bulk parameterization of air-sea fluxes: Updates and verification for the COARE algorithm, *J. Clim.*, *16*, 571–591.
- Fewings, M. R., and S. J. Lentz (2011), Summertime cooling of the shallow continental shelf, *J. Geophys. Res.*, *116*, C07015, doi:10.1029/2010JC006744.
- Fofonoff, N. P. and R. C. Millard Jr. (1983), Algorithms for computation of fundamental properties of seawater, *UNESCO Tech. Pap. Mar. Sci.*, *44*, 53 pp.
- Grebmeier, J. M., Overland, J. E., Moore, S. E., Farley, E. V., Carmack, E. C., Cooper, L. W., Frey, K. E., Helle, J. H., McLaughlin, F. A., and McNutt, S. L. (2006), A major ecosystem shift in the northern Bering Sea, *Science*, *311* 1461–1466.
- Hare, S. R., and N. J. Mantua (2000), Empirical evidence for North Pacific regime shifts in 1977 and 1989, *Prog. Oceanogr.*, *47*(2–4), 103–146.
- Hermann, A. J., S. Hinckley, E. L. Dobbins, D. B. Haidvogel, N. A. Bond, C. Mordy, N. Kachel and P. J. Stabeno (2009), Quantifying cross-shelf and vertical nutrient flux in the Gulf of Alaska with a spatially nested, coupled biophysical model, *Deep Sea Res., Part II*, *56*, 2474–2486, doi:10.1016/j.dsr2.2009.02.008.
- Hunt, G. L., Coyle, K. O., Eisner, L., Farley, E. V., Heintz, R., Mueter, F., Napp, J. M., Overland, J. E., Ressler, P. H., Salo, S., Stabeno, P. J. (2011), Climate impacts on eastern Bering Sea food webs: a synthesis of new data and an assessment of the Oscillating Control Hypothesis, *ICES J. Mar. Sci.*, doi:10.1093/icesjms/fsr036.
- Janout, M. A., T. J. Weingartner, S. L. Okkonen, T. Whitledge, and D. L. Musgrave (2009), Some characteristics of Yakutat Eddies propagating along the continental slope of the northern Gulf of Alaska, *Deep Sea Res., Part II*, *56*, 2444–2459.
- Janout, M. A., T. J. Weingartner, T. C. Royer, and S. L. Danielson (2010), On the nature of winter cooling and the recent temperature shift on the northern Gulf of Alaska shelf, *J. Geophys. Res.*, *115*, C05023, doi:10.1029/2009JC005774.
- Johnson, W. R., T. C. Royer, and J. L. Luick (1988), On the seasonal variability of the Alaska Coastal Current, *J. Geophys. Res.*, *93*(C10), 12423–12437.
- Kalnay, E., et al. (1996), The NCEP/NCAR 40-year reanalysis project, *Bull. Am. Meteorol. Soc.*, *77*, 437471.
- Lackmann, G. M., and J. Overland (1989), Atmospheric structure and momentum balance during a gapwind event in Shelikof Strait, Alaska, *Mon. Weather Rev.*, *117*, 1817–1833.
- Ladd, C., and N. A. Bond (2002), Evaluation of NCEP/NCAR reanalysis in the NE Pacific and the Bering Sea, *J. Geophys. Res.*, *107*(C10), 3158.
- Ladd, C., P. J. Stabeno, and E. D. Cokelet (2005), A note on cross-shelf exchange in the northern Gulf of Alaska, *Deep Sea Res., Part II*, *52*, 667–679.
- Lentz, S. J. (1987), A heat budget for the northern California shelf during CODE 2, *J. Geophys. Res.*, *92*, 14,491–14,509.
- Lentz, S. J. (2010), The mean along-isobath heat and salt balances over the Middle Atlantic Bight continental shelf, *J. Phys. Oceanogr.*, *40*, 934–948.
- Lentz, S. J., R. K. Shearman, and A. J. Plueddemann (2010), Heat and salt balances over the New England continental shelf, August 1996 to June 1997, *J. Geophys. Res.*, *115*, C07017, doi:10.1029/2009JC006073.
- Liu, H., P. Q. Olsson, K. P. Volz, and H. Yi (2006), A climatology of mesoscale model simulated low-level wind jets over Cook Inlet and Shelikof Strait, Alaska, *Estuar. Coast. Shelf Sci.*, *70*, 551–566.
- Loescher, K. A., G. S. Young, B. A. Colle, and N. S. Winstead (2006), Climatology of barrier jets along the Alaskan coast. Part I: Spatial and temporal distributions, *Mon. Weather Rev.*, *134*, 437–453.
- Macklin, S. A., G. M. Lackmann, and J. Gray (1988), Offshore-directed winds in the vicinity of Prince William Sound, Alaska, *Mon. Weather Rev.*, *116*, 1289–1301.
- Macklin, S. A., N. A. Bond, and J. P. Walker (1990), Structure of a low-level jet over lower Cook Inlet, Alaska, *Mon. Weather Rev.*, *118*(12), 2568–2578.
- Mantua, N. J., S. R. Hare, Y. Zhang, J. M. Wallace, and R. C. Francis (1997), A Pacific interdecadal climate oscillation with impacts on salmon production, *Bull. Am. Meteorol. Soc.*, *78*(6), 1069–1080.
- Mesinger, et al. (2006), North American Regional Reanalysis, *Bull. Am. Meteorol. Soc.*, *87*, 343–360, doi:10.1175/BAMS-87-3-343.
- Niebauer, H. J., T. C. Royer, and T. J. Weingartner (1994), Circulation of Prince William Sound, Alaska, *J. Geophys. Res.*, *99*, 14,113–14,126.
- Overland, J. E., and T. R. Hiester (1980), Development of a synoptic climatology for the Northeast Gulf of Alaska, *J. Appl. Meteorol.*, *19*, 1–14.
- Overland, J. E., and N. A. Bond (1993), The influence of coastal orography: The Yakutat storm, *Mon. Weather Rev.*, *121*, 1388–1397.
- Reed, R. K., and P. J. Stabeno (2002), Surface heat fluxes and subsurface heat content at a site over the southeastern Bering Sea shelf, May–July 1996, *Deep Sea Res., Part II*, *49*(26), 5911–5917, doi:10.1016/S0967-0645(02)00325-9.
- Richman, J. G., and A. Badan-Dangon (1983), Mean heat and momentum budgets during upwelling for the coastal waters off northwest Africa, *J. Geophys. Res.*, *88*, 2626–2632.
- Rodionov, S. N., N. A. Bond, and J. E. Overland (2007), The Aleutian Low, storm tracks, and winter climate variability in the Bering Sea, *Deep Sea Res., Part II*, *54*, 2560–2577.
- Royer, T. C. (1981), Baroclinic transport in the Gulf of Alaska, Part II: Freshwater driven coastal current, *J. Mar. Res.*, *39*, 251–266.
- Royer, T. C. (1982), Coastal freshwater discharge in the Northeast Pacific, *J. Geophys. Res.*, *87*(C3), 2017–2021.
- Royer, T. C. (2005), Hydrographic responses at a coastal site in the northern Gulf of Alaska to seasonal and interannual forcing, *Deep Sea Res., Part II*, *52* (1–2), 267–288.
- Royer T. C., and C. E. Grosch (2006), Ocean warming and freshening in the northern Gulf of Alaska, *Geophys. Res. Lett.*, *33*, L16605, doi:10.1029/2006GL026767.
- Rudnick, D. L., and R. E. Davis (1988), Mass and heat budgets on the northern California continental shelf, *J. Geophys. Res.*, *93*, 14013–14024.
- Sarkar, N., T. C. Royer and C. E. Grosch (2005), Hydrographic and mixed layer depth variability on the shelf in the northern Gulf of Alaska, 1974–1998, *Cont. Shelf Res.*, *25*, 2147–2162.
- Schumacher, J. D., P. J. Stabeno, and A. T. Roach (1989), Volume transport in the Alaska Coastal Current, *Cont. Shelf Res.*, *9*, 1071–1083.
- Smith, R. D., J. K. Dukowicz, and R. C. Malone (1992), Parallel ocean general circulation modeling, *Physica D*, *60*, 38–61.
- Spall, M. A. (2007), Circulation and water mass transformation in a model of the Chukchi Sea, *J. Geophys. Res.*, *112*, C05025, doi:10.1029/2005JC002264.
- Stabeno, P. J., R. K. Reed and J. D. Schumacher (1995), The Alaska Coastal Current: continuity of transport and forcing, *J. Geophys. Res.*, *100*(C2), 2477–2485.
- Stabeno, P. J., R. K. Reed, and J. M. Napp (2002), Transport through Unimak Pass, Alaska, *Deep Sea Res., Part II*, *49*, 5919–5930.
- Stabeno, P. J., N. A. Bond, A. J. Hermann, N. B. Kachel, C. W. Mordy, and J. E. Overland (2004), Meteorology and oceanography of the northern Gulf of Alaska, *Cont. Shelf Res.*, *24*, 859–897.
- Stabeno, P. J., D. G. Kachel, N. B. Kachel, and M. E. Sullivan (2005), Observations from moorings in the Aleutian Passes: Temperature, salinity and transport, *Fish. Oceanogr.*, *14*(Suppl. 1), 39–54, doi:10.1111/j.1365-2419.2005.00362.x.
- Trenberth, and Hurrell (1994), Decadal atmosphere-ocean variations in the Pacific, *Clim. Dyn.*, *9*, 303–319.

- Weingartner, T. J., et al. (2002), The Northeast Pacific GLOBEC Program: Coastal Gulf of Alaska, *Oceanography*, 15, 48–63.
- Weingartner, T. J., S. L. Danielson, and T. C. Royer (2005), Freshwater variability and predictability in the Alaska Coastal Current, *Deep Sea Res., Part II*, 52, 169–191.
- Weingartner, T., E. Dobbins, S. Danielson, P. Winsor, R. Potter, and H. Statscewich (2013), Hydrographic variability over the northeastern Chukchi Sea shelf in summer–fall 2008–2010, *Cont. Shelf Res.*, in press.
- Williams, W. J., T. J. Weingartner, and A. J. Herrmann (2007), Idealized three-dimensional modeling of seasonal variation in the Alaska Coastal Current, *J. Geophys. Res.*, 112, C07001, doi:10.1029/2005JC003285.
- Wilson, J. G., and J. E. Overland (1986), Meteorology, in *The Gulf of Alaska, Physical Environment and Biological Resources*, edited by D. W. Hood, and S. T. Zimmerman, pp. 31–53, Alaska Office, Ocean Assessments Division, National Oceanic and Atmospheric Administration, U.S. Department of Commerce.
- Woodgate, R. A., K. Aagaard, and T. J. Weingartner (2005), Monthly temperature, salinity, and transport variability of the Bering Strait through flow, *Geophys. Res. Lett.* 32, L04601, doi:10.1029/2004GL021880.
- Woodgate, R. A., T. J. Weingartner, and R. Lindsay (2010), The 2007 Bering Strait oceanic heat flux and anomalous Arctic sea ice retreat, *Geophys. Res. Lett.* 37, L01602, doi:10.1029/2009GL041621.